JOURNAL OF PROPULSION AND POWER
Vol. 21, No. 1, January–February 2005

Numerical and Experimental Investigation of the Current Distribution in Self-Field Magnetoplasmadynamic Thrusters

Jörg Heiermann* and Monika Auweter-Kurtz†
Universität Stuttgart, 70550 Stuttgart, Germany

The plasma flow in magnetoplasmadynamic (MPD) self–field thrusters is described by conservation equations for heavy particles, turbulence, electrons, and the magnetic field for reaction and thermal nonequilibrium. The equations are discretized on unstructured adaptive meshes. The numerical results, which are verified by experimental data, show that the newly developed finite volume code predicts the thrust well. It is found that electron pressure diffusion drives the arc out of nozzle-type MPD thrusters. The drop of density in front of a water-cooled anode is the reason for the beginning of thruster instabilities at high electric currents.

Nomenclature

$\boldsymbol{B}$	=	magnetic field, T
C	=	turbulent closure coefficient
c	=	speed of sound, ms^{-1}
$\boldsymbol{E}$	=	electric field, Vm^{-1}
e	=	energy density, Jm^{-3}
e	=	constant 1.60219×10^{-19} A · s
F	=	flux, $\mathrm{m}^{-2}\mathrm{s}^{-1}$
F	=	force, N
f	=	near-wall function
$\boldsymbol{f}$	=	momentum flux, Nm^{-2}
$\boldsymbol{f}$	=	energy flux, Wm^{-2}
h	=	splitting quantity, ms^{-1}
I	=	current, A
$\boldsymbol{j}$	=	diffusion flux, $\mathrm{m}^{-2}\mathrm{s}^{-1}$
$\boldsymbol{j}$	=	electric current density, Am^{-2}
k	=	reaction rate, $\mathrm{m}^3\mathrm{s}^{-1}$
k	=	constant 1.38062×10^{-23} J · K^{-1}
m_h	=	constant 6.63349×10^{-26} kg
$\dot{m}$	=	mass flux, kg s^{-1}
n	=	particle density, m^{-3}
$\mathcal{P}$	=	turbulent production term, $\mathrm{m}^2\mathrm{s}^{-3}$
p	=	pressure, Pa
q	=	source term, Nm^{-3} and Wm^{-3}
q	=	velocity, ms^{-1}
R	=	turbulent conservation quantity, $\mathrm{m}^2\mathrm{s}^{-1}$
r	=	radial coordinate, m
s	=	reference velocity, ms^{-1}
T	=	temperature, K
t	=	time, s
U	=	voltage, V
$\boldsymbol{v}$	=	velocity, ms^{-1}
Z	=	charge number
z	=	axial coordinate, m
α	=	parameter
α	=	energy transfer coefficient, $\mathrm{Wm}^{-3}\mathrm{K}$
β	=	Hall parameter, $\mathrm{m}^3\mathrm{C}^{-1}$
γ	=	adiabatic coefficient ($\frac{5}{3}$)
ε	=	small number (10^{-20})
λ	=	eigenvalue, ms^{-1}
λ	=	thermal conductivity, $\mathrm{Wm}^{-1}\mathrm{K}^{-1}$
μ	=	dynamic viscosity, $\mathrm{kg}^{-1}\mathrm{m}^{-1}\mathrm{s}^{-1}$
μ_0	=	constant $4\pi \times 10^{-7}$ V · $\mathrm{sA}^{-1}\mathrm{m}^{-1}$
ν	=	kinematic viscosity, $\mathrm{m}^2\mathrm{s}^{-1}$
ξ	=	mass fraction
ρ	=	density, $\mathrm{kg}^{-3}\mathrm{m}^{-3}$
σ	=	turbulent closure coefficient
σ	=	electric conductivity, $\Omega^{-1}\mathrm{m}^{-1}$
τ	=	viscous stress, Nm^{-2}
φ	=	azimuthal
χ	=	ionization energy, J
$\boldsymbol{\Psi}$	=	molar fraction
$\boldsymbol{\Psi}$	=	stream function, Tm
ω	=	nonlinear weight
ω	=	reaction source term, $\mathrm{m}^{-3}\mathrm{s}^{-1}$

Subscripts

A	=	anode
b	=	backward
C	=	cathode
D	=	diffusion
e	=	electron
f	=	forward
h	=	heavy particle
i	=	i-fold ionized species
in	=	inflow
invisc	=	inviscid
$j \times B$	=	Lorentz force
n	=	normal
P	=	plasma
r	=	radial
T	=	turbulent
$\mathcal{T}$	=	triangle
visc	=	viscous
z	=	axial
$\varepsilon, \varepsilon_1, \varepsilon_2$	=	turbulent closure coefficient

Presented as Paper 2001-3498 at the AIAA/ASME/SAE/ASEE 37th Joint Propulsion Conference and Exhibit, Salt Lake City, UT, 8–11 July 2001; received 15 September 2003; accepted for publication 23 August 2004.

*Research Engineer, Institut für Raumfahrtsysteme, Pfaffenwaldring 31; heierman@irs.uni-stuttgart.de. Member AIAA.

†Professor, Institut für Raumfahrtsysteme, Pfaffenwaldring 31. Associate Fellow AIAA.

Introduction

MAGNETOPLASMADYNAMIC (MPD) self-field thrusters are candidates for propelling manned spacecraft to Mars because they can achieve a high exhaust velocity combined with a high thrust density.[1–3]

Since the early 1980s, MPD thrusters have been investigated at the Institut für Raumfahrtsysteme (IRS) experimentally,[4,5] theoretically,[6,7] and numerically.[8–10] Engineering apects[11,12] as well as basic plasma processes[13–15] are considered to achieve higher

efficiency and to avoid power-limiting instabilities. Reasons for thruster instabilities, which are identified by voltage oscillations and increasing anode losses,[16] are the depletion of the charged particle density at the anode,[17] microturbulence[18,19] and space charge, drift, and gradient-driven instabilities.[20,21]

For more than three decades, numerical methods and codes have been developed worldwide,[22–28] with the complexity of the discretized conservation equations increasing with the available computing power. To investigate plasma flows in self-field MPD thrusters, a new finite volume solver has been written for solving the conservation equations describing a continuum–mechanical, turbulent axisymmetric argon plasma flow under the influence of an arc discharge in thermal and reaction nonequilibrium on adaptive, unstructured meshes.

In the following sections, the conservation equations will be presented, some important aspects of the discretization will be discussed, and results for the plasma source RD3 and the MPD thruster DT2, both of which have been developed and are being operated in the IRS laboratory, will be shown.

Conservation Equations

Conservation of Mass

The mass conservation equations for i-fold charged argon particles can be written as conservation equations for their densities:

$$\frac{\partial n_i}{\partial t} = -\mathrm{div}(n_i \boldsymbol{v}) - \mathrm{div}\boldsymbol{j}_{D,i} + \omega_i, \qquad i = 0, \ldots, 6 \tag{1}$$

With the total heavy particle density

$$n_h = \sum_{i=0}^{6} n_i \tag{2}$$

the mass fraction[29]

$$\xi_i = n_i / n_h \tag{3}$$

the molar fraction[29]

$$\Psi_i = n_i / (n_h + n_e) \tag{4}$$

the diffusion flux[30–32]

$$\boldsymbol{j}'_{D,i} = -n_h D_{im} \nabla \Psi_i \tag{5}$$

and the requirement of mass conservativity, the diffusion flux becomes[33]

$$\boldsymbol{j}_{D,i} = \boldsymbol{j}'_{D,i} - \xi_i \sum_{k=0}^{6} \boldsymbol{j}'_{D,k} \tag{6}$$

The reaction source term ω_i describes the production of ions and electrons by electron impact ionization[34,35] and the neutralization of ions by three-body recombination,[9]

$$\begin{aligned}
\omega_0 &= -n_0 n_e k_{f,1} + n_1 n_e^2 k_{b,1} \\
\omega_i &= -n_i n_e k_{f,i+1} + n_{i+1} n_e^2 k_{b,i+1} \\
&\quad - n_i n_e^2 k_{b,i} + n_{i-1} n_e k_{f,i}, \qquad i = 1 \ldots 5 \\
\omega_6 &= -n_6 n_e^2 k_{b,6} + n_5 n_e k_{f,6}
\end{aligned} \tag{7}$$

Conservation of Momentum

The conservation equation for the axial momentum is

$$\frac{\partial(\rho v_z)}{\partial t} = -\mathrm{div}\boldsymbol{f}_{z,\mathrm{invisc}} - \mathrm{div}\boldsymbol{f}_{z,\mathrm{visc}} \tag{8}$$

with the inviscid flux

$$\boldsymbol{f}_{z,\mathrm{invisc}} = \begin{bmatrix} p_h + p_e + \dfrac{B^2}{2\mu_0} + \rho v_z^2 \\ \rho v_z v_r \end{bmatrix} \tag{9}$$

and the viscous flux

$$\boldsymbol{f}_{z,\mathrm{visc}} = \begin{bmatrix} -\tau_{zz} \\ -\tau_{zr} \end{bmatrix} \tag{10}$$

The conservation of radial momentum is given by

$$\frac{\partial(\rho v_r)}{\partial t} = -\mathrm{div}\boldsymbol{f}_{r,\mathrm{invisc}} - \mathrm{div}\boldsymbol{f}_{r,\mathrm{visc}} + q_r \tag{11}$$

with the inviscid flux

$$\boldsymbol{f}_{r,\mathrm{invisc}} = \begin{bmatrix} \rho v_z v_r \\ p_h + p_e + \dfrac{B^2}{2\mu_0} + \rho v_r^2 \end{bmatrix} \tag{12}$$

and the visous flux

$$\boldsymbol{f}_{r,\mathrm{visc}} = \begin{bmatrix} -\tau_{zr} \\ -\tau_{rr} \end{bmatrix} \tag{13}$$

The source term

$$q_r = \left[p_h + p_e - \tau_{\varphi\varphi} - \left(B^2 / 2\mu_0 \right) \right] / r \tag{14}$$

is caused by the use of cylindrical coordinates.[36,37]

The viscous stresses are[38]

$$\begin{aligned}
\tau_{zz} &= \frac{2}{3}(\mu_h + \mu_T)\left(2\frac{\partial v_z}{\partial z} - \frac{v_r}{r} - \frac{\partial v_r}{\partial r} \right) \\
\tau_{zr} &= (\mu_h + \mu_T)\left(\frac{\partial v_z}{\partial r} + \frac{\partial v_r}{\partial z} \right) \\
\tau_{rr} &= \frac{2}{3}(\mu_h + \mu_T)\left(2\frac{\partial v_r}{\partial r} - \frac{v_r}{r} - \frac{\partial v_z}{\partial z} \right) \\
\tau_{\varphi\varphi} &= \frac{2}{3}(\mu_h + \mu_T)\left(2\frac{v_r}{r} - \frac{\partial v_r}{\partial r} - \frac{\partial v_z}{\partial z} \right)
\end{aligned} \tag{15}$$

Conservation of Heavy Particle Energy

The conservation equation for the heavy particle energy

$$\frac{\partial e_h}{\partial t} = -\mathrm{div}\boldsymbol{f}_{h,\mathrm{invisc}} - \mathrm{div}\boldsymbol{f}_{h,\mathrm{visc}} + q_h \tag{16}$$

includes the inviscid flux

$$\boldsymbol{f}_{h,\mathrm{invisc}} = \left(e_h + p_h + p_e + \frac{B^2}{2\mu_0} \right) \begin{bmatrix} v_z \\ v_r \end{bmatrix} \tag{17}$$

the viscous flux

$$\boldsymbol{f}_{h,\mathrm{visc}} = \begin{bmatrix} -\tau_{zz} v_z - \tau_{zr} v_r - (\lambda_h + \lambda_T)\dfrac{\partial T_h}{\partial z} \\ -\tau_{zr} v_z - \tau_{rr} v_r - (\lambda_h + \lambda_T)\dfrac{\partial T_h}{\partial r} \end{bmatrix} \tag{18}$$

and the source term

$$q_h = \left(p_e + \frac{B^2}{2\mu_0} \right) \mathrm{div}\,\boldsymbol{v} - \frac{B^2}{\mu_0 r} v_r + \sum_{i=0}^{6} n_e n_i \alpha_{ei} (T_e - T_h) \tag{19}$$

The heavy particle energy e_h, when assuming the equation of state

$$p_h = n_h k T_h \tag{20}$$

is composed of translatory and kinetic energy,

$$e_h = \tfrac{3}{2} n_h k T_h + \tfrac{1}{2} \rho |\boldsymbol{v}|^2 \tag{21}$$

The diffusion flux of enthalpy

$$\sum_{i=0}^{6} \left(\frac{5}{2} k T_h + \frac{1}{2} m_h |\boldsymbol{v}|^2 \right) \boldsymbol{j}_{D,i}$$

is zero because of the aforementioned requirement of mass conservative diffusion, and thus, it does not appear in Eq. (16).

Conservation of Turbulence

The conservation equation for the turbulent conservation quantity ρR is[39,40]

$$\frac{\partial(\rho R)}{\partial t} = -\mathrm{div}(\rho R\boldsymbol{v}) + \mathrm{div}\left[\rho\left(\nu_h + \frac{\nu_T}{\sigma_\varepsilon}\right)\nabla R\right] + \rho(C_{\varepsilon 2} f_2 - C_{\varepsilon 1})\sqrt{R\mathcal{P}} - \nabla\left[\rho\left(\nu_h + \frac{\nu_T}{\sigma_\varepsilon}\right)\right]\cdot\nabla R - \frac{\rho}{\sigma_\varepsilon}\nabla\nu_T\cdot\nabla R \tag{22}$$

The turbulent production term is written in cylindrical coordinates as

$$\mathcal{P} = \nu_T\left\{2\left[\left(\frac{\partial v_z}{\partial z}\right)^2 + \left(\frac{\partial v_r}{\partial r}\right)^2 + \left(\frac{v_r}{r}\right)^2\right] + \left(\frac{\partial v_z}{\partial r} + \frac{\partial v_r}{\partial z}\right)^2 - \frac{2}{3}\left(\frac{\partial v_z}{\partial z} + \frac{\partial v_r}{\partial r} + \frac{v_r}{r}\right)^2\right\} \tag{23}$$

The closure coefficients and the near–wall functions may be found in Ref. 39.

Conservation of Electron Energy

The electron pressure p_e and the electron energy e_e are defined by

$$p_e = n_e k T_e \tag{24}$$

$$e_e = \tfrac{3}{2} n_e k T_e \tag{25}$$

Because of quasi-neutrality, the electron density n_e is

$$n_e = \sum_{i=1}^{6} Z_i n_i \tag{26}$$

The conservation equation of electron energy is given by

$$\frac{\partial e_e}{\partial t} = -\mathrm{div}(e_e\boldsymbol{v}) - p_e\mathrm{div}\,\boldsymbol{v} + \frac{5}{2}\frac{k}{e}\boldsymbol{j}\cdot\nabla T_e - \frac{1}{en_e}\boldsymbol{j}\cdot\nabla p_e - \mathrm{div}\left(\frac{3}{2}kT_e\sum_{i=1}^{6} Z_i\boldsymbol{j}_{D,i}\right) + \mathrm{div}(\lambda_e\nabla T_e) + \sum_{i=0}^{6} n_e n_i \alpha_{ei}(T_h - T_e) + \frac{|j|^2}{\sigma} - \sum_{i=0}^{5}\omega_{i+1}\chi_{i\to i+1} \tag{27}$$

Conservation of Magnetic Field

With Ohm's law for plasmas (see Ref. 41),

$$\boldsymbol{E} = (\boldsymbol{j}/\sigma) - \boldsymbol{v}\times\boldsymbol{B} + \beta\boldsymbol{j}\times\boldsymbol{B} - \beta\nabla p_e \tag{28}$$

and the Hall parameter

$$\beta = 1/en_e \tag{29}$$

the Maxwell equations of classical electrodynamics (see Ref. 42) can be written as one conservation equation for the azimuthal magnetic field component B,

$$\frac{\partial B}{\partial t} = -\mathrm{div}(B\boldsymbol{v}) + \frac{Bv_r}{r} - \mathrm{rot}\left(\frac{\mathrm{rot}\,\boldsymbol{B}}{\mu_0\sigma} + \frac{\beta}{\mu_0}\,\mathrm{rot}\,\boldsymbol{B}\times\boldsymbol{B} - \beta\nabla p_e\right)_\varphi \tag{30}$$

The first term on the right-hand side of Eq. (30) represents the convective transport of the magnetic field; the second is caused by the use of cylindrical coordinates. The third term describes the time-dependent change of the magnetic field by the electric current $\boldsymbol{j}$ that flows through the plasma of the conductivity σ, by the Hall current, and by the electron pressure diffusion.

In Eq. (30) the magnetic field B can be substituted by the stream function

$$\Psi = rB \tag{31}$$

In steady state, a constant electric current flows between two contour lines of the stream function Ψ.

Reaction Rates and Transport Coefficients

The forward reaction rates $k_{f,i}$ are computed with the formulas from Ref. 34, 35, and 43; the reaction equilibrium constants[44] that are needed for the calculation of the backward reaction rates $k_{b,i}$ (principle of detailed equilibrium) are computed with the data found in Refs. 45–47.

Based on the model of electrostatic microfields,[48,49] the collision cross sections are calculated with the Gvosdover formula (see Refs. 9, 50, and 51) taking into account the Debye shielding length (see Ref. 41). For collisions with neutral particles, data given in Ref. 52 are used. The transport coefficients like viscosity or electron thermal conductivity are then computed following Refs. 6, 10, and 53–60.

The forward reaction rates $k_{f,i}$, the particle densities n_i (for reaction and thermal equilibrium) and the transport coefficients are shown in Figs. 1–8.

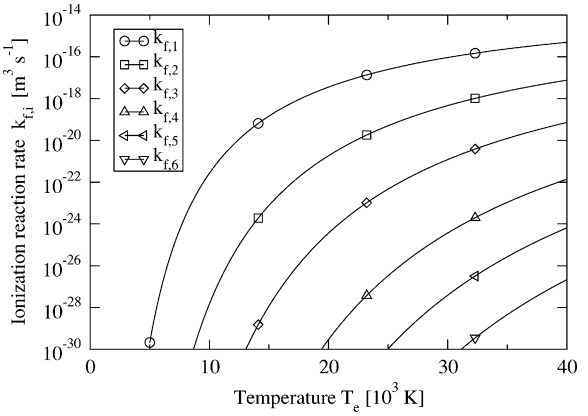

Fig. 1 Reaction rates $k_{f,i}$ for argon.

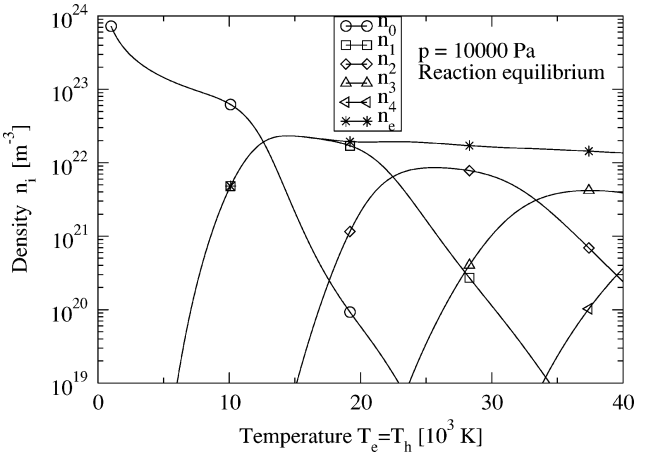

Fig. 2 Particle densities n_i.

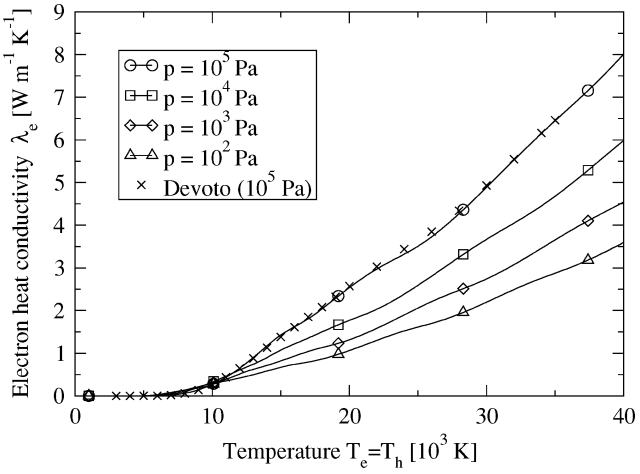

Fig. 3 Electron thermal conductivity λ_e.

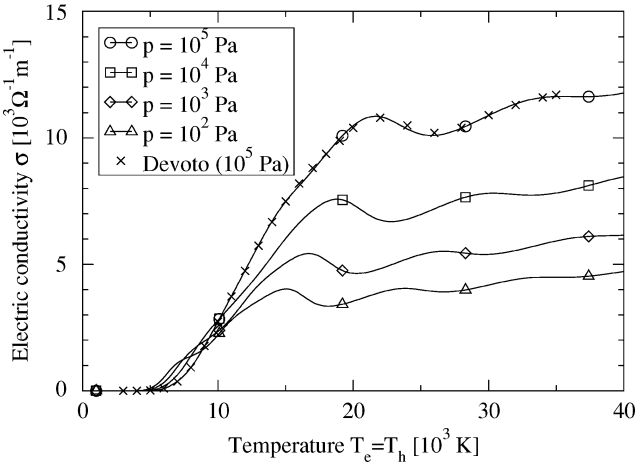

Fig. 4 Electric conductivity σ.

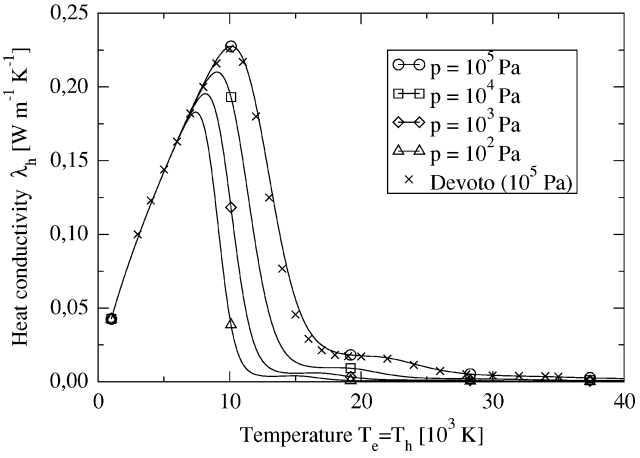

Fig. 5 Thermal conductivity λ_h.

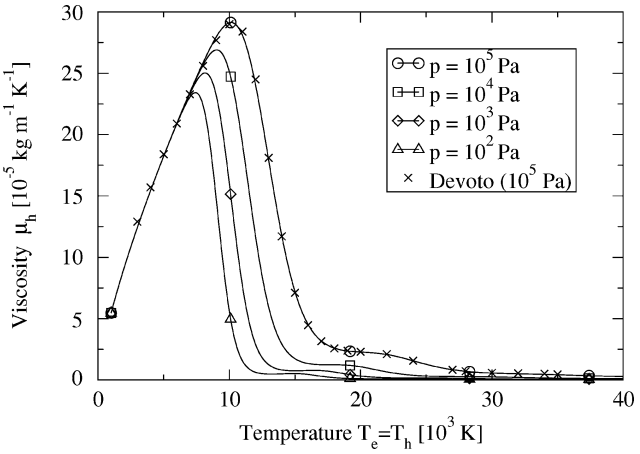

Fig. 6 Viscosity μ_h.

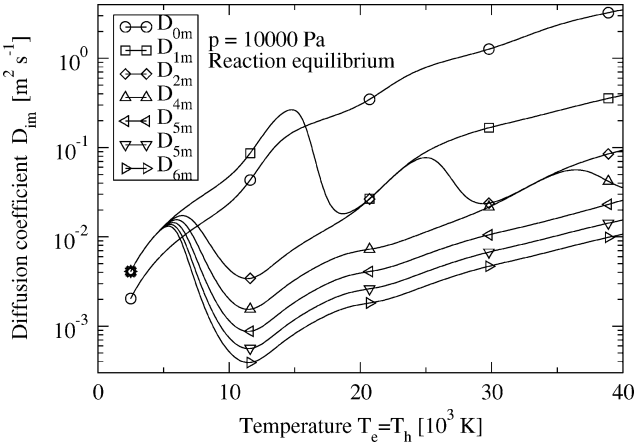

Fig. 7 Diffusion coefficient D_{im}.

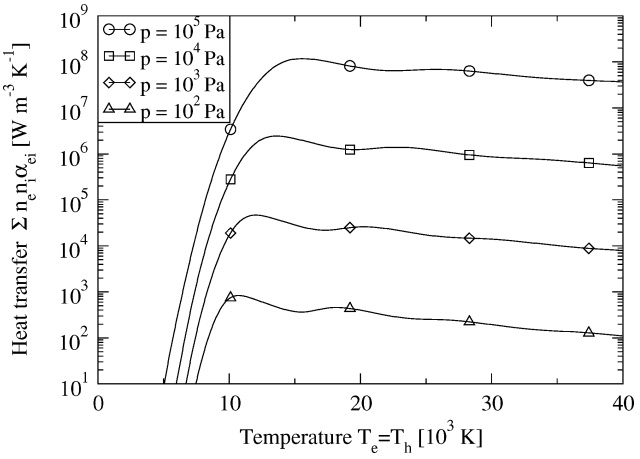

Fig. 8 Heat transfer $\sum n_e n_i \alpha_{ei}$.

Boundary Conditions

On the inflow boundary, the prescribed mass flow with a temperature of 500 K is kept constant by a numerical mass flow controller. The heavy particles' temperature is set to a preselected wall temperature (500 K for all water-cooled electrodes and neutral thruster segments), and their velocity is zero on all solid walls. On the outflow boundary, subsonic and supersonic outflow are distinguished, as well as artificial inflow at 1 Pa, which simulates a possible recirculation of rest gas in the laboratory tank. The electrons are assumed to behave adiabatic on all boundaries. The electric field vector only has a component perpendicular to the electrode surfaces, and everywhere else Ampère's law is applied.

Numerical Methods

The computational domain is discretized with a mesh consisting of triangles produced by an advancing front algorithm. Then, dual cells are constructed, with their corners being in the centers of the triangles. These dual cells represent the toroidal control volumes, which contain the average values of all of the variables.

To achieve second-order accuracy, the variables needed to compute the inviscid fluxes through the cell faces of the dual cells have

to be reconstructed linearly on each cell. This is accomplished by a weighted essentially nonoscillatory (WENO) scheme,[61] which is described here for the density ρ as an example: As a nonlinear weight for the gradient $(\nabla\rho)_{\mathcal{T}_j}$ on one of the triangles $\mathcal{T}_j$ associated with a dual cell i, one computes

$$\omega_j = \frac{\left(\varepsilon + \rho_{z,j}^2 + \rho_{r,j}^2\right)^{-2}}{\sum_{k=1}^{J}\left(\varepsilon + \rho_{z,k}^2 + \rho_{r,k}^2\right)^{-2}} \tag{32}$$

Then, the WENO gradient for the dual cell i is given by

$$(\nabla\rho)_i^{\mathrm{WENO}} = \sum_{j=1}^{J} \omega_j (\nabla\rho)_{\mathcal{T}_j} \tag{33}$$

where J denotes all of the triangles associated with the dual cell i. This reconstruction algorithm can be implemented easily on unstructured as well as on structured meshes, and it proves to be very robust.

The inviscid fluxes are computed by a flux vector splitting scheme.[62] Because the magnetic field is always perpendicular to the flow velocity vector, the speed of sound is given by the magnetoacoustic wave:

$$c = \sqrt{\gamma(p_h + p_e)/\rho + B^2/\mu_0\rho} \tag{34}$$

Now, a new reference velocity is defined:

$$s = \sqrt{\alpha c^2 + q^2[1 - 2\alpha + \alpha(q^2/c^2)]} \tag{35}$$

with

$$q^2 = \min\left(c^2, q_n^2\right) \tag{36}$$

The velocity normal to a cell face of two neighboring dual cells is

$$q_n = v_z n_z + v_r n_r \tag{37}$$

The eigenvalues are now defined by

$$\lambda_0 = q_n, \qquad \lambda_1 = \lambda_0 + s, \qquad \lambda_2 = \lambda_0 - s \tag{38}$$

With the states left (l) and right (r) of a cell face the following ansatz is made for the mass flux splitting:

$$h_{1l} = \tfrac{1}{4}(\lambda_{1l} + |\lambda_{1l}|) \tag{39}$$

$$h_{1r} = \tfrac{1}{4}(\lambda_{1r} - |\lambda_{1r}|) \tag{40}$$

$$h_{2l} = \tfrac{1}{4}(\lambda_{2l} + |\lambda_{2l}|) \tag{41}$$

$$h_{2r} = \tfrac{1}{4}(\lambda_{2r} - |\lambda_{2r}|) \tag{42}$$

For example, the species density flux is now computed as

$$F_{\mathrm{invisc}}^{n_i} = n_{il}(h_{1l} + h_{1r}) + n_{ir}(h_{2l} + h_{2r}) \tag{43}$$

The parameter α is chosen in such a way that in the case of vanishing (macroscopic) normal velocity q_n the single-sided mass flux equals the effusion flux $n_h\bar{c}/4$ of the particles, which leads to

$$\alpha = 2/\gamma\pi \tag{44}$$

The parabolic fluxes are evaluated on each triangle with Cramer's rule so that their discretization has a quasi-central character (see Refs. 63 and 64). Other differentials are approximated by the least-square method.

In the finite volume context, the theorems of Gauß and Stokes are used extensively to assure a maximum of conservativity in the numerical code.

Time-stabilization of steady state is relatively quickly achieved with explicit, first-order, randomized local time steps.[65]

Results

Plasma source RD3

To investigate the arc attachment on water–cooled copper anodes the flow in the plasma source RD3, which is used in the IRS plasma wind tunnels and for plasma material coating, has been simulated for an argon mass flow rate of 2.4 g/s. Figure 9 shows a typical adapted mesh for an electric current of 2000 A.

For 1000 A (Fig. 10), most of the arc attaches on the anode backface. This is caused exclusively by electron pressure diffusion, which drives the arc out of the diverging nozzle. This strong influence was checked by switching the electron pressure diffusion term in Ohm's law for plasmas on and off in numerical experiments.

For 2000 A (Fig. 11), part of the arc attaches on the inner side of the anode. This inner region of the anode was covered with ceramics in the experiment (Fig. 12). The voltage/current in Fig. 13 shows no influence of the ceramics cover for 1000 A, whereas a voltage difference of 5 V can be seen for 2000 A where the ceramics cover obviously blocks the arc attachment so that a higher voltage has to pull the arc either in front of or behind the ceramics cover onto the noncovered anode surface. Thus, the correctness of the numerically predicted arc attachment on the water-cooled anode of the RD3 was verified by the experiment.

Yet another phenomenon can be explained by the numerical simulation, namely, the occasional appearance of small burning spots on the anode backface. Here, the electron temperature (Fig. 14) drops rapidly due to the expansion of the plasma flow after the nozzle exit area. The charged particle density and the electric conductivity

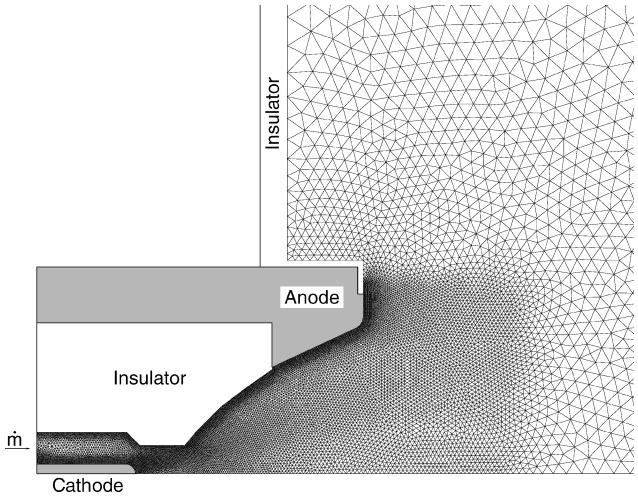

Fig. 9 Adapted mesh for plasma source RD3, 2000 A, 2.4 g/s argon.

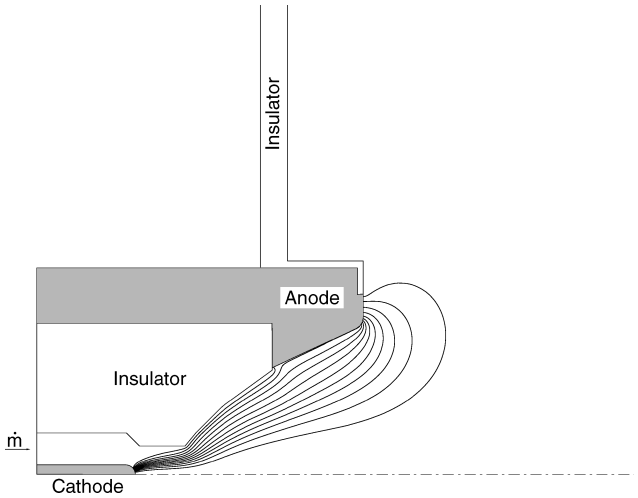

Fig. 10 Current distribution RD3, 1000 A, 2.4 g/s argon (100 A between two isolines).

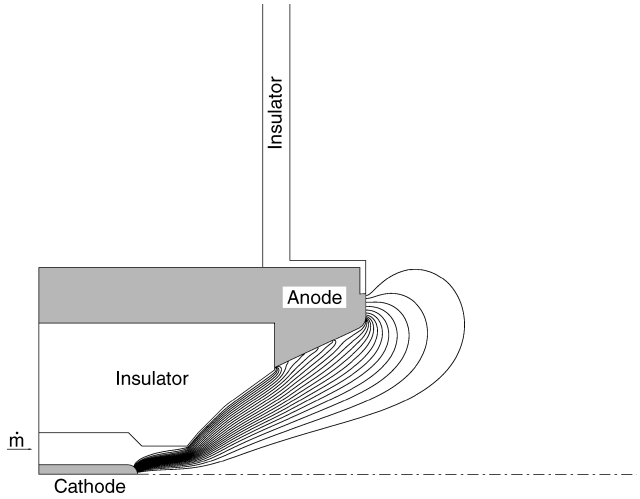

Fig. 11 Current distribution RD3, 2000 A, 2.4 g/s argon (100 A between two isolines).

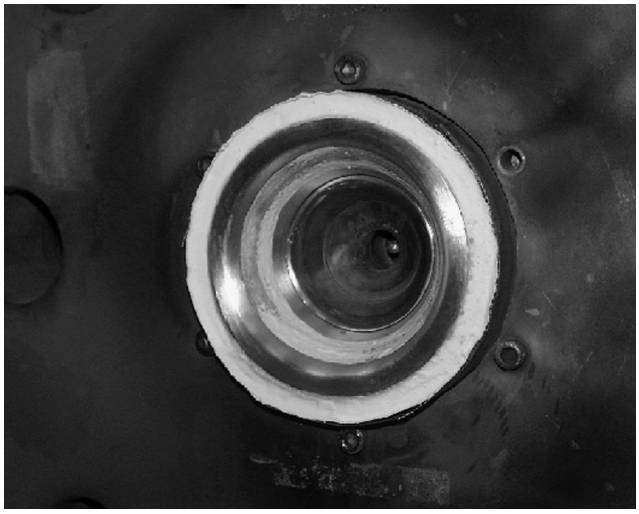

a) RD3 in vacuum tank

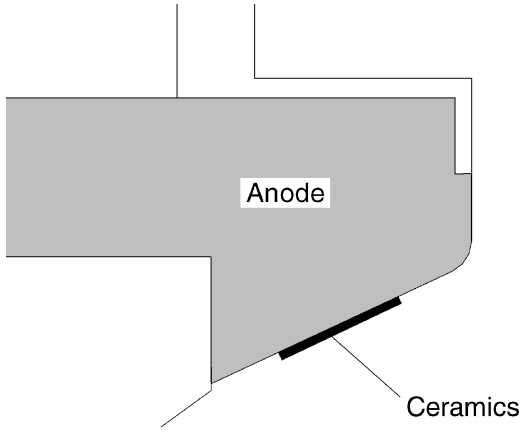

b) Scheme of ceramics cover

Fig. 12 RD3 with ceramics cover on anode.

drop accordingly so that only a sporadic spotty arc attachment with a locally increased electric field is able to sustain the total current.

MPD Thruster DT2

The MPD thruster DT2 is a generic design for the examination of MPD thrusters with diverging nozzles. Diverging nozzles are used to convert thermal energy into kinetic energy so that thermal thrust is produced in addition to the electromagnetic thrust.

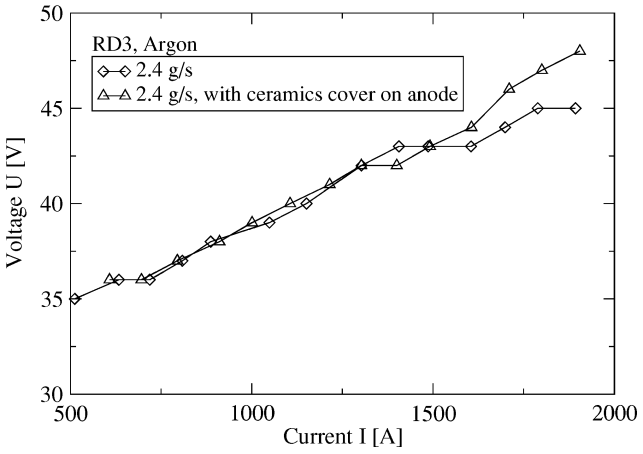

Fig. 13 Voltage vs current RD3, with and without ceramics cover.

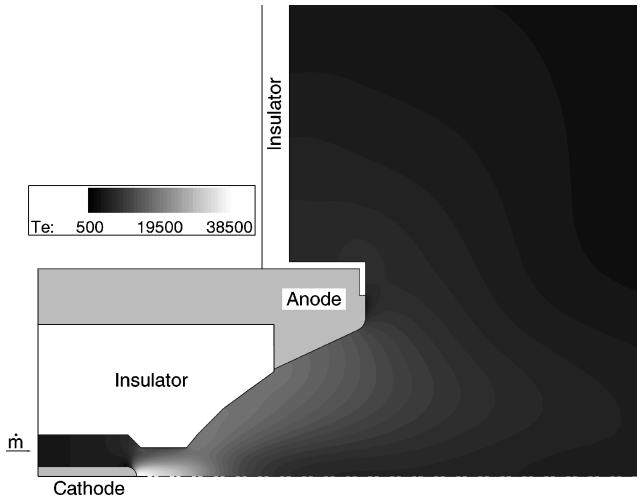

Fig. 14 Electron temperature T_e RD3, 2000 A, 2.4 g/s argon.

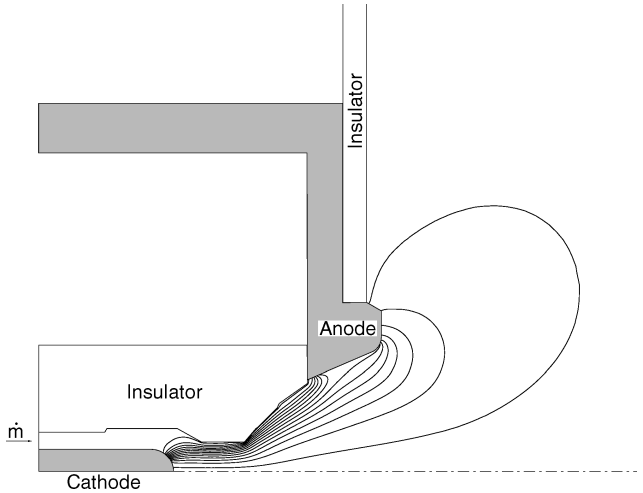

Fig. 15 Current distribution Ψ DT2, 3000 A, 0.8 g/s argon (250 A between two isolines).

Electron pressure diffusion drives the arc out of the nozzle (Figs. 15–17). With the current increasing from 3000 to 5000 A, the pinch effect becomes the dominating mechanism to control the flow properties in the diverging nozzle. The arc constricts (Figs. 15–17) so that a drastic decrease in density becomes evident in front of the anode (Figs. 18–20). This strong drop of density is the main reason for the start of thruster instabilities because the current cannot be sustained because of the lack of charged particles. In the

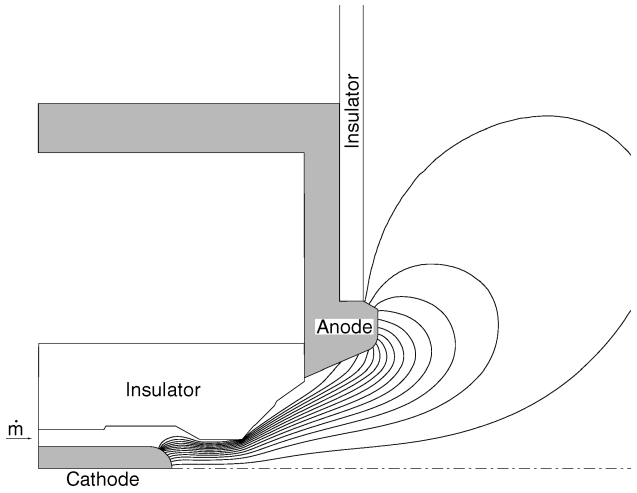

Fig. 16 Current distribution Ψ DT2, 4000 A, 0.8 g/s argon (250 A between two isolines).

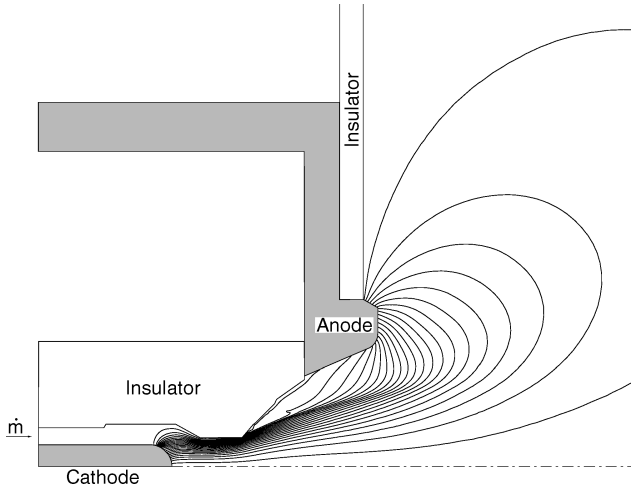

Fig. 17 Current distribution Ψ DT2, 5000 A, 0.8 g/s argon (250 A between two isolines).

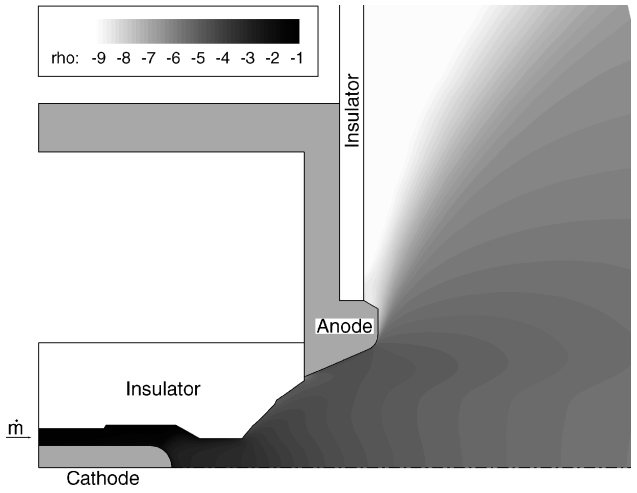

Fig. 18 Density $\log_{10}\rho$ DT2, 3000 A, 0.8 g/s argon.

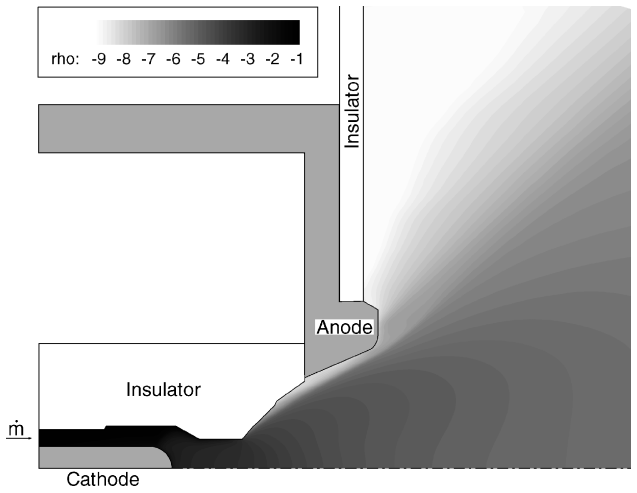

Fig. 19 Density $\log_{10}\rho$ DT2, 4000 A, 0.8 g/s argon.

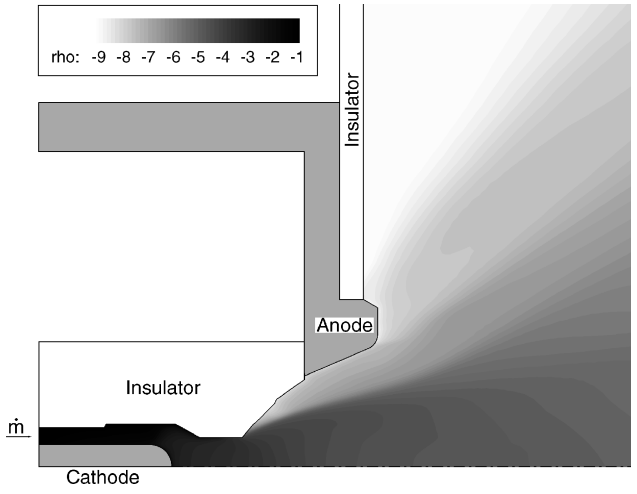

Fig. 20 Density $\log_{10}\rho$ DT2, 5000 A, 0.8 g/s argon.

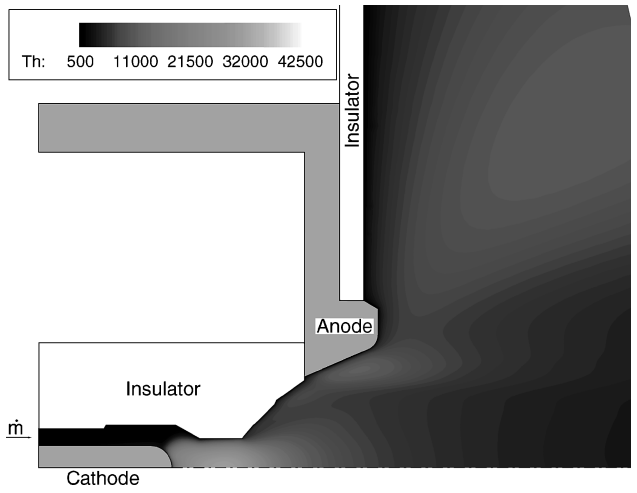

Fig. 21 Heavy particle temperature T_h DT2, 3000 A, 0.8 g/s argon.

experiment (mass flow rate 0.8 g/s), a current of 4000 A can only be sustained safely with additional anode gas, whereas strong oscillations occur for 4650 A so that a current of 5000 A cannot be achieved.[5] The numerical code is able to predict the density drop in front of the anode and, thus, the beginning of thruster instabilities correctly.

Also, the prediction of inlet pressure and thrust (Table 1) agrees nicely with experimental data. The numerical determination of the anode and cathode voltage U_A and U_C remains to be done by implementing appropriate electrode models.

Whereas the increase of the heavy particle temperature in front of the anode is caused by an oblique shock for 3000 A (Fig. 21), the increase of T_h for 4000 and 5000 A (Figs. 22 and 23) clearly coincides with the sharp density drop. This effect should also be investigated experimentally.

Again, like for the RD3, the electron temperature (Figs. 24–26) drops near the anode backface, which is the reason for sporadic spotty arc attachment.

Table 1 Inlet pressure, voltage, thrust DT2

I, A	$\dot{m}$, g/s	p_{in}, kPa		U_P, V,	U_{C+P+A}, V,	$F_{j\times B}$, N,	F, N	
		Numerical	Experimental[5]	numerical	experimental[5]	numerical	Numerical	Experimental[5]
2000	0,8	7,6	7,8	28,1	36,2	0,8	4,3	4,6
3000	0,8	9,2	9,5	33,5	45,6	1,8	5,8	6,2
4000	0,8	10,3	10,7	43,8	55,9	3,1	7,1	8,3
5000	0,8	12,7	——	53,9	——	5,0	8,2	——

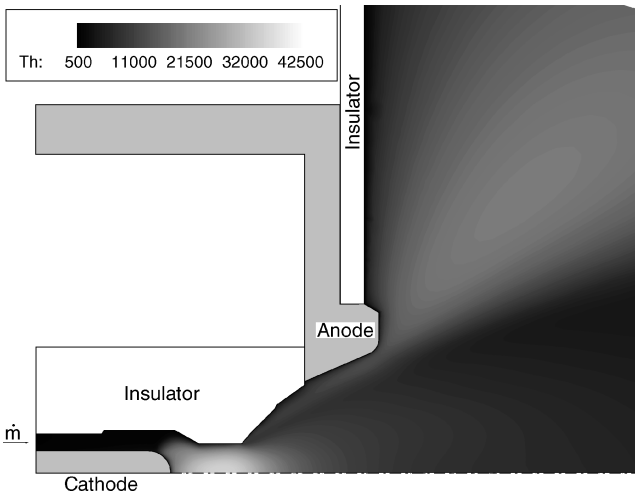

Fig. 22 Heavy particle temperature T_h DT2, 4000 A, 0.8 g/s argon.

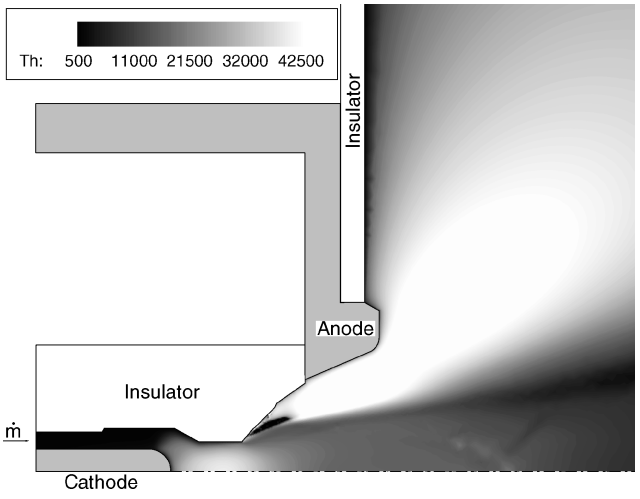

Fig. 23 Heavy particle temperature T_h DT2, 5000 A, 0.8 g/s argon.

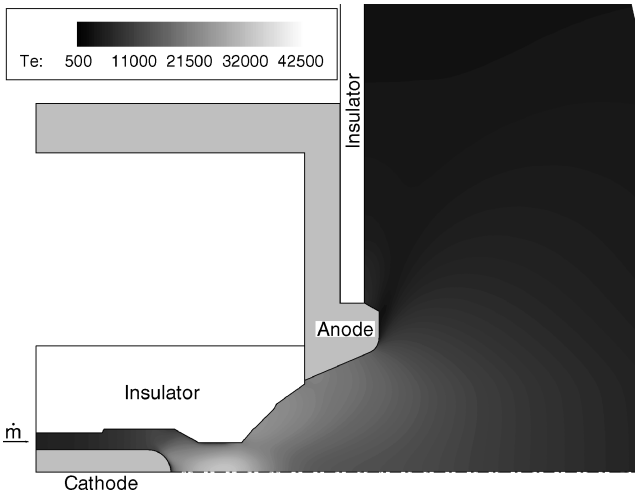

Fig. 24 Electron temperature T_e DT2, 3000 A, 0.8 g/s argon.

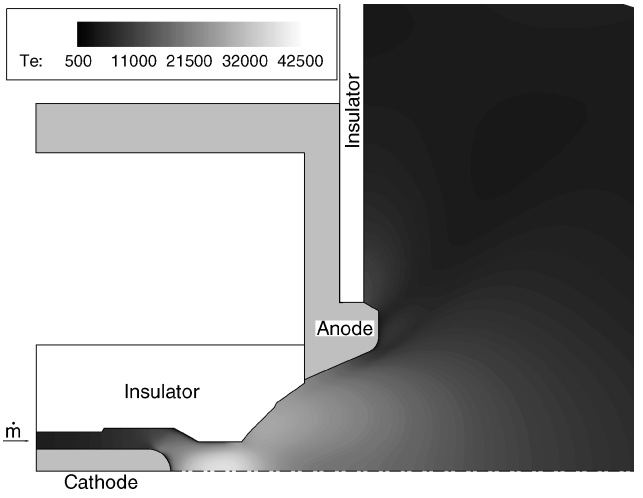

Fig. 25 Electron temperature T_e DT2, 4000 A, 0.8 g/s argon.

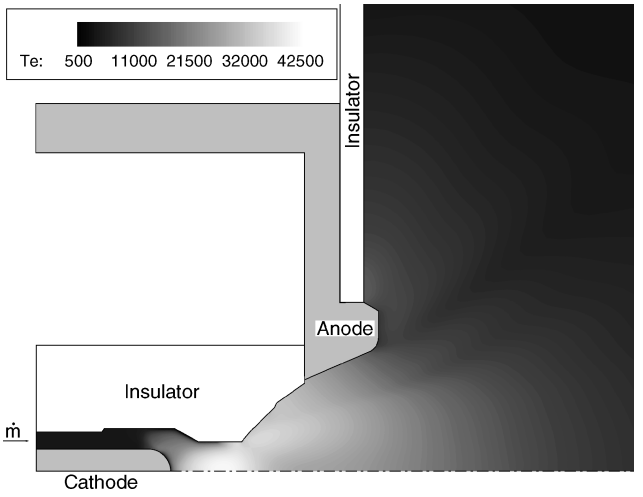

Fig. 26 Electron temperature T_e DT2, 5000 A, 0.8 g/s argon.

Conclusions

It has been shown that the arc in nozzle-type MPD thrusters is driven out of the nozzle by electron pressure diffusion. This was predicted numerically with a new finite volume code and verified experimentally for the plasma source RD3.

The strong decrease of density in front of the water-cooled anode due to the pinch effect has been computed in detail for the MPD thruster DT2. This density drop is the main reason for the start of thruster instabilities found in the experiment.

The decrease of electron temperature has been found to be the reason for sporadic spotty arc attachement on the backface of water-cooled anodes.

The new code also predicts the thrust well so that it can be used for the design of MPD thrusters. The thruster geometry can now be optimized with respect to maximum thrust and efficiency while shifting the start of instabilites to higher currents.

For the prediction of the overall voltage, electrode models will be implemented in the next step.

Acknowledgments

This work has been supported by the German Research Foundation Deutsche Forschungsgemeinschaft through project Conservation Equations and Numerical Solutions for Technically Relevant Magneto-Plasmas (Au 85/9-1,2), which belongs to the German Priority Research Program (Schwerpunktprogramm) Analysis and Numerics for Conservation Laws. The authors especially thank C.A. Coclici and H.J. Kaeppeler for their outstanding support.

References

[1]Jahn, R. G., *Physics of Electric Propulsion*, Missile and Space Technology Series, McGraw–Hill, New York, 1968, Chap. 1.

[2]Auweter-Kurtz, M., *Lichtbogenantriebe für Weltraumaufgaben*, B. G. Teubner, Stuttgart, Germany, 1992, Chap. 7.

[3]Bennett, G. L., Watkins, M. A., Byers, D. C., Barnett, J. W., "Enhancing Space Transportation: The NASA Program to Develop Electric Propulsion," International Electric Propulsion Conf., Paper IEPC-90-004, July 1990.

[4]Wegmann, T., "Experimentelle Untersuchung kontinuierlich betriebener magnetoplasmadymamischer Eigenfeldtriebwerke," Ph.D. Dissertation, Inst. für Raumfahrtsysteme, Fakultät für Luft-und Raumfahrttechnik, Univ. of Stuttgart, Stuttgart, Germany, 1994.

[5]Auweter-Kurtz, M., Boie, C., Habiger, H., Kaeppeler, H. J., Kurtz, H. L., Sleziona, P. C., Wegmann, T., and Winter, M. W., "Numerische Simulation von MPD–Triebwerken und Vergleich mit durchzuführenden experimentellen Untersuchungen," Endbericht zum DFG–Forschungsvorhaben Au85/5-2, Inst. für Raumfahrtsysteme, Univ. of Stuttgart, Stuttgart, Germany 1998.

[6]Wagner, H. P., "Theoretische Untersuchung drift- und gradientengetriebener Instabilitäten in MPD–Triebwerksströmungen," Ph.D. Dissertation, Inst. für Raumfahrtsysteme, Fakultät Luft- und Raumfahrttechnik, Univ. of Stuttgart, Stuttgart, Germany, 1994.

[7]Kaeppeler, H. J., "Basic Equations and Elements of the Dispersion Relation for a Four-Fluid Formalism of Magneto-Plasmadynamics with Non-equilibrium Ionization," International Electric Propulsion Conf., Paper IEPC-91-059, Oct. 1991.

[8]Sleziona, P. C., "Numerische Analyse der Strömungsvorgänge in magnetoplasmadynamischen Raumfahrtantrieben," Ph.D. Dissertation, Inst. für Raumfahrtsysteme, Fakultät Luft- und Raumfahrttechnik, Univ. of Stuttgart, Stuttgart, Germany, 1992.

[9]Sleziona, P. C., "Hochenthalpieströmungen für Raumfahrtanwendungen," Habilitation Thesis, Habilitationsschrift, Fakultät Luft- und Raumfahrttechnik, Univ. of Stuttgart, Stuttgart, Germany, 1998.

[10]Boie, C., "Numerische Simulation magnetoplasmadynamischer Eigenfeldtriebwerke mit hochauflösenden adaptiven Verfahren," Ph.D. Dissertation, Inst. für Raumfahrtsysteme, Fakultät Luft- und Raumfahrttechnik, Univ. of Stuttgart, Stuttgart, Germany, 1999.

[11]Bühler, R. D., "Plasma thruster development: magnetoplasmadynamic propulsion, status and basic problems," U.S. Air Force Rocket Propulsion Lab., AFRPL TR-86-013, Edwards AFB, CA, 1986.

[12]Auweter-Kurtz, M., "Plasma Thruster Development Program at the IRS," *Acta Astronautica*, Vol. 32, No. 5, 1994, pp. 377–391.

[13]Auweter-Kurtz, M., "Zur Dynamik der mit Kaltgas angeströmten Lichtbogensäule," Ph.D. Dissertation, Inst. für Raumfahrtantriebe, Fakultät Luft– und Raumfahrttechnik, Univ. of Stuttgart, Stuttgart, Germany, 1985.

[14]Schrade, H. O., "Basic Processes of Plasma Propulsion," Interim Scientific Rept., U.S. Air Force Office of Scientific Research Grant 82-0298, Inst. für Raumfahrtsysteme, Univ. of Stuttgart, Stuttgart, Germany, 1982.

[15]Schrade, H. O., "Basic Processes of Plasma Propulsion," Interim Scientific Report, U.S. Air Force Office of Scientific Research Grant 86-0337, Inst. für Raumfahrtsysteme, Univ. of Stuttgart, Stuttgart, Germany, 1987.

[16]Merke, W. D., Auweter-Kurtz, M., Habiger, H., Kurtz, H. L., and Schrade, H. O., "Nozzle Type MPD Thruster Experimental Investigations," International Electric Propulsion Conf., Paper IEPC-88-028, Oct. 1988.

[17]Hügel, H., "Zur Funktionsweise der Anode im Eigenfeldbeschleuniger," Habilitation, Fakultät für Luft- und Raumfahrttechnik, DFVLR Forschungsbericht 80-20, Univ. of Stuttgart, Stuttgart, Germany, 1980.

[18]Choueiri, E. Y., "Electron–Ion Streaming Instabilities of an Electromagnetically Accelerated Plasma," Ph.D. Dissertation, Princeton Univ., Princeton, NJ, 1991.

[19]Choueiri, E. Y., "Anomalous Resistivity and Heating in Current-Driven Plasma Thrusters," *Physics of Plasmas*, Vol. 6, No. 5, 1999, pp. 2290–2306.

[20]Wagner, H. P., Kaeppeler, H. J., and Auweter-Kurtz, M., "Instabilities in MPD Thruster Flows: 1. Space Charge Instabilities in Unbounded and Inhomogeneous Plasmas," *Journal of Physics D: Applied Physics*, Vol. 31, No. 5, March 1998, pp. 519–528.

[21]Wagner, H. P., Kaeppeler, H. J., and Auweter-Kurtz, M., "Instabilities in MPD Thruster Flows: 2. Investigation of Drift and Gradient Driven Instabilities Using Multi–Fluid Plasma Models," *Journal of Physics D: Applied Physics*, Vol. 31, No. 5, 1998, pp. 529–541.

[22]Hügel, H., "Zur Strömung kompressibler Plasmen im Eigenfeld von Lichtbogenentladungen," Ph.D. Dissertation, Inst. für Plasmadynamik der Deutschen Versuchsanstalt für Luft– und Raumfahrt, DFVLR Forschungsbericht 70–13, 1970.

[23]Minakuchi, H., and Kuriki, K., "Magnetoplasmadynamic Analysis of Plasma Acceleration," International Electric Propulsion Conf., Paper IEPC-84-06, May 1984.

[24]Niewood, E. H., and Martinez-Sanchez, M., "A Two Dimensional Model of an MPD Thruster," AIAA Paper 91-2344, June 1991.

[25]Turchi, P. J., Mikellides, P. G., Hohman, K. W., Leiweke, R. J., Mikellides, I. G., Schmahl, C. S., Roderick, N. F., and Peterkin, R. E., Jr., "Progress in Modeling Plasma Thrusters and Related Plasma Flows," International Electric Propulsion Conf., Paper IEPC-95-159, Sept. 1995.

[26]Fujita, K., "Performance Computation of a Low–Power Hydrogen Arcjet," AIAA Paper 96-3183, July 1996.

[27]Sankaran, K., Choueiri, E. Y., and Jardin, S. C., "Application of a New Numerical Solver to the Simulation of MPD Flows," AIAA Paper 2000-3537, July 2000.

[28]Sankaran, K., "Simulation of MPD Flows Using a Flux–Limited Numerical Method for the MHD Equations," M.Sc. Dissertation 3074-T, Dept. of Mechanical and Aerospace Engineering, Princeton Univ., Princeton, NJ, Jan. 2001.

[29]Frohn, A., *Einführung in die Technische Thermodynamik*, AULA-Verlag, Wiesbaden, Germany, 1989, Chap. 3.

[30]Hirschfelder, J. O., Curtiss, C. F., and Bird, R. B., *Molecular Theory of Gases and Liquids*, Wiley, New York, 1967, Chaps. 7, 8.

[31]Yos, J. M., "Transport Properties of Nitrogen, Hydrogen, Oxygen, and Air to 30000 K," Technical Memorandum RAD-TM-63-7, Aeronautical Systems Div., U.S., Air Force Systems Command, Wright–Patterson AFB, Ohio, 1963.

[32]Fertig, M., Dohr, A., and Frühauf, H.-H., "Transport Coefficients for High Temperature Nonequilibrium Air Flows," AIAA Paper 98-2937, June 1998.

[33]Sutton, A., and Gnoffo, P. A., "Multi-Component Diffusion with Application to Computational Aerothermodynamics," AIAA Paper 98-2575, June 1998.

[34]Lotz, W., "An Empirical Formula for the Electron-Impact Ionization Cross-Section," *Zeitschrift für Physik*, Vol. 206, 1967, pp. 205–211.

[35]Lotz, W., "Electron-Impact Ionization Cross–Sections and Ionization Rate Coefficients for Atoms and Ions from Hydrogen to Calcium," *Zeitschrift für Physik*, Vol. 216, 1968, pp. 241–247.

[36]Trostel, R., *Vektor– und Tensoranalysis*, Vieweg, 1997.

[37]Oevermann, M., "Ein Finite–Volumen–Verfahren auf unstrukturierten Dreiecksgittern zur Berechnung turbulenter Diffusionsflammen in kompressiblen Strömungsfeldern," Ph.D. Dissertation, Rheinisch-Westfälische Technische Hochschule Aachen, Aachen, Germany, 1997.

[38]Schlichting, H., and Gersten, K., *Grenzschicht–Theorie*, Springer-Verlag, Berlin, 1997.

[39]Goldberg, U. C., and Ramakrishnan, S. V., "A Pointwise Version of Baldwin–Barth Turbulence Model," *Computational Fluid Dynamics*, Vol. 1, 1993, pp. 321–338.

[40]Wilcox, D. C., *Turbulence Modeling for CFD*, DCW Industries, La Canada, CA, 1993, Chap. 4.

[41]Cap, F., *Lehrbuch der Plasmaphysik und Magnetohydrodynamik*, Springer-Verlag, Berlin, 1994, Chap. 6.

[42]Greiner, W., *Theoretische Physik*, Klassische Elektrodynamik, Vol. 3, Verlag Harri Deutsch, 1991, Chap. 4.

[43]Lotz, W., "Subshell Binding Energies of Atoms and Ions from Hydrogen to Zinc," *Journal of the Optical Society of America*, Vol. 58, No. 7, 1968, pp. 915–921.

[44]Unsöld, A., *Physik der Sternatmosphähren*, Springer-Verlag, Berlin, Pt. 1, 1968, Chap. 4.

[45]Drawin, H.-W., and Felenbrok, P., *Data for Plasmas in Local Thermodynamic Equilibrium*, Gauthiers–Villars, 1965.

[46]Landau, L. D., and Lifshitz, E. M., *Quantum Mechanics*, Pergamon, Oxford, 1958, Chap. 8.

[47]Moore, C. E., "Atomic Energy Levels," Rept. NSRDS-NBS 35, Vol. 1, National Bureau of Standards, 1947.

[48]Kaeppeler, H. J., "Equilibrium and Non-Equilibrium Thermodynamics of Plasma Flow," Goodyear Aircraft Corp., Rept. GER 10930, 1963.

[49]Baumann, G., "Zur quantenmechanischen Statistik von Gasen und reagierenden Gasgemischen," Ph.D. Dissertation, Inst. für Physik der Strahlantriebe, Univ. of Stuttgart, Stuttgart, Germany, 1956.

[50]Finkelnburg, W., and Maecker, H., *Elektrische Bögen und thermisches Plasma*, Handbuch der Physik, Vol. 22, Gasentladungen II, Springer-Verlag, Berlin, 1956, pp. 343–350.

[51]Schrade, H. O., Bez, W., Höcker, K. H., and Kaeppeler, H. J., "Zur Theorie der Ohm'schen Heizung vollionisierter Plasmen," *Zeitschrift für Naturforschung*, Vol. 15a, No. 2, 1960.

[52]Devoto, R. S., "Transport Coefficients of Ionized Argon," *Physics of Fluids*, Vol. 16, No. 5, 1973, pp. 616–623.

[53]Kaeppeler, H. J., and Baumann, G., "Irreversible Stochastic Thermodynamics and the Transport Phenomena in a Reacting Plasma," Mitteilungen aus dem Forschungsinstitut für Strahlantriebe, Rept. 8, Stuttgart, Germany, 1956.

[54]Schrade, H. O., Sleziona, P. C., Wegmann, T., and Kurtz, H. L., "Basic Processes of Plasma Propulsion," Interim Scientific Rept., U.S. Air Force Office of Scientific Research, Grant 91-0118, Inst. für Raumfahrtsysteme, Univ. of Stuttgart, Stuttgart, Germany, 1992.

[55]Devoto, R. S., "Transport Coefficients of High Pressure Argon in a Magnetic Field," Aerospace Research Labs., Rept. ARL 71-0075, Air Force Systems Command, Wright–Patterson AFB, Ohio, April 1971.

[56]Nazarenko, I. P., and Panevin, I. G., "Simple Method for Calculating Transport Properties of Electrons in Argon Plasma," *High Temperature Journal*, Vol. 27, No. 3, 1989 (translation from *Teplofhisika vysokih temperatur*).

[57]Nikrityuk, P. A., "Mathematical Modelling of the Gas Heating in the Hydrogen Arcjet," Ph.D. Dissertation, Moscow State Aviation Inst., Moscow, 1999.

[58]Lee, J.-H., "Basic Governing Equations for the Flight Regimes of Aeroassisted Orbital Transfer Vehicles," Progress in Aeronautics and Astronautics, Thermal Design of Aeroassisted Orbital Transfer Vehicles, edited by H. E. Nelson, Vol. 96, AIAA, Washington, DC, 1985, pp. 3–53.

[59]Morse, T. F., "Energy and Momentum Exchange between Nonequipartition Gases," *Physics of Fluids*, Vol. 6, 1963, pp. 1420–1427.

[60]Park, C., *Nonequilibrium Hypersonic Aerothermodynamics*, Wiley, New York, 1990, Chap. 4.

[61]Friedrich, O., "Weighted Essentially Non-Oscillatory Schemes for the Interpolation of Mean Values on Unstructured Grids," *Journal of Computational Physics*, Vol. 144, No. 1, 1998, pp. 194–212.

[62]Heiermann, J., Auweter-Kurtz, M., Kaeppeler, H. J., Eberle, A., Iben, U., and Sleziona, P. C., "Recent Improvements of Numerical Methods for the Simulation of MPD Thruster Flow on Adaptive Meshes," *Proceedings of the 26th International Electric Propulsion Conference*, Oct. 1999, pp. 964–969; also IEPC-99-169.

[63]Meister, A., "Zur zeitgenauen numerischen Simulation reibungsbehafteter, kompressibler, turbulenter Strömungsfelder mit einer impliziten Finite–Volumen–Methode vom Box–Typ," Ph.D. Dissertation, Fachbereich Mathematik der Technischen Hochschule Darmstadt, 1996.

[64]Hannemann, V., "Numerische Simulation von Stoß–Stoß–Wechselwirkungen unter Berücksichtigung von chemischen und thermischen Nichtgleichgewichtseffekten," DLR–Forschungsbericht 97-07, DLR, Inst. für Strömungsmechanik, Göttingen, Germany, 1997.

[65]Heiermann, J., Auweter-Kurtz, M., Coclici, C., Munz, C.-D., and Sleziona, P. C., "Magnetoplasmadynamic Rocket Thruster Simulation," *Proceedings of the Eighth International Conference on Hyperbolic Problems: Theory, Numerics, Applications*, edited by H. Freistühler and G. Warnecke, Birkhäuser Verlag, Magdeburg, Germany, 2001, pp. 99–108.